JOURNAL OF CATALYSIS 78, 360–379 (1982)

Photoacoustic Spectroscopy Study of Metal–Support Interactions in $Co/\gamma\text{-}Al_2O_3$ and $Ni/\gamma\text{-}Al_2O_3$ Catalysts

L. W. BURGGRAF[1] AND D. E. LEYDEN[2]

Department of Chemistry, University of Denver, Denver, Colorado 80208

AND

ROLAND L. CHIN AND DAVID M. HERCULES

University of Pittsburgh, Pittsburgh, Pennsylvania 15260

Received January 7, 1982; revised June 8, 1982

Series of $Ni/\gamma\text{-}Al_2O_3$, $Co/\gamma\text{-}Al_2O_3$, and $Co\text{–}Mo/\gamma\text{-}Al_2O_3$ catalysts which were previously studied by various surface spectroscopy techniques were examined using photoacoustic spectroscopy. Metal–support interactions were found to increase with decreasing metal loading and increasing calcination temperature, in agreement with surface spectroscopy results. Metal oxides segregate on the surface at high metal loading. The qualitative dependence of the tetrahedral metal ion fraction and octahedral metal ion fraction on metal loading and calcination temperature is explained by a simple model. The model describes the competition between bulk tetrahedral metal ion formation and inversion of the spinel at the surface of the support.

INTRODUCTION

Catalysis by metals and metal oxides is a much-studied field of chemistry. Because of the industrial importance of these materials, a large body of empirical knowledge about catalytic phenomena has been accumulated. However, the empirical practice of heterogeneous catalysis has preceded understanding of the nature of catalyst surfaces. Surface spectroscopy techniques have recently made important contributions to the understanding of the influence of preparation parameters on the catalyst surface. This study adds photoacoustic spectroscopy to the list of spectroscopic techniques which have been applied to the investigation of supported metal oxide catalysts demonstrating the value of photoacoustic spectroscopy for qualitative and quantitative study of catalyst surfaces.

Alumina-supported nickel and cobalt catalysts have been widely studied because of their catalytic activity in industrially important reactions, especially hydrocracking, hydrogenation, and methanation. Moreover, knowledge of alumina-supported cobalt catalysts may ultimately be extended to provide a better insight into the nature of alumina-supported cobalt–molybdenum catalysts which are particularly important in catalytic hydrodesulfurization of crude petroleum. Hercules and co-workers (*1–4*) have employed a variety of surface spectroscopy techniques to study metal–support interactions in $Ni/\gamma\text{-}Al_2O_3$ and $Co/\gamma\text{-}Al_2O_3$ catalysts. X-Ray photoelectron spectroscopy (ESCA), ion scattering spectroscopy (ISS), and extended X-ray absorption fine structure spectroscopy (EXAFS) were employed to investigate the change in surface species as a function of metal loading and calcination temperature. In the case of the $Co/\gamma\text{-}Al_2O_3$ system, secondary ion mass spectrometry (SIMS) was also used to help characterize surface species (*4*). Re-

[1] Present address: Department of Chemistry, HQ USAFA/DFC, USAF Academy, Colo. 80840.

[2] To whom correspondence should be sent.

0021-9517/82/120360-20$02.00/0

cent popularization of photoacoustic spectroscopy (PAS) prompted its application to the study of these catalyst systems. The primary objective of this study was to use PAS to confirm and, if possible, to extend the results of surface spectroscopic investigations of γ-alumina-supported metal oxide catalysts using the same samples which were characterized by surface spectroscopy.

EXPERIMENTAL

Catalyst samples were prepared by members of the Pittsburgh research group. Details of catalyst preparation and characterization of Co/γ-Al_2O_3 and Ni/γ-Al_2O_3 catalysts have been reported previously (*1, 2, 4*). The γ-alumina (Alpha-Ventron, 90 m^2/g) used as a support for catalysts was prepared by grinding until the powder passed through a 200-mesh sieve. The nickel and cobalt catalysts were made by impregnation of the powdered γ-alumina with aqueous solutions of reagent-grade $Ni(NO_3)_2$ or $Co(NO_3)_2$, drying at 110°C, and calcining in air for 5 h. These catalyst samples were prepared with various bulk metal loadings using calcination temperatures in the range 400 to 600°C. The Co–Mo/γ-Al_2O_3 catalyst samples were prepared by sequential impregnation of γ-Al_2O_3 with molybdenum and cobalt. The γ-Al_2O_3 (Harshaw, 190 m^2/g) was prepared by grinding it and then passing the powder through a 100-mesh sieve. The resulting material was dried overnight at 110°C. An aqueous solution of $(NH_4)_6Mo_7O_{24} \cdot 9H_2O$ was mixed with the prepared γ-alumina. This mixture was dried at 110°C overnight. Molybdenum-impregnated γ-alumina was calcined at 550°C in air for 16 h. Samples of the molybdenum-loaded alumina were mixed with aqueous solutions of $Co(NO_3)_2$. Then the drying and calcination steps were repeated. The amount of molybdenum loaded on the support was found to be within ±1% Mo of the calculated value; the amount of cobalt loaded on the support was found to be within ±0.3% Co of the calculated value.

Samples of pure materials were obtained for comparison with catalyst samples. When necessary these materials were physically diluted with the γ-alumina used in catalyst preparation. Before use the γ-alumina was dried at 80°C in a vacuum oven. When mixing with γ-alumina was inadequate to yield a uniform sample, the mixture was found for 3 min in a miniature stainless-steel ball mill. Samples of $Ni(NO_3)_2 \cdot 6H_2O$ (Baker), $Co(NO_3)_2 \cdot 6H_2O$ (Mallinckrodt), $CoAl_2O_4$ (CERAC), and Co_3O_4 (Pfaltz and Bauer) were prepared by grinding with γ-alumina. The $NiAl_2O_4$ samples were made by heating a mixture of $Ni(NO_3)_2$ and γ-alumina at 1300°C. The $NiAl_2O_4$ materials were not so optically absorbent as to require dilution. NiO (Baker, gray-black) was powdered by calcining at 600°C for 5 h. Quantitative dilutions of this material were made by mixing with γ-alumina. The octahedral component of a cobalt oxide sample was enhanced by heating powdered Co_3O_4 at 1100 ± 15°C for 11 h and then cooling the material under vacuum. Although the stoichiometry of the resulting material is uncertain, the octahedral Co(II) component is enhanced. A sample of $CoMoO_4$ (Pfaltz and Bauer) was prepared by dilution with γ-alumina for comparison with Co–Mo/γ-Al_2O_3 samples.

The photoacoustic spectrometer used in these studies has been described previously, as have the data analysis method and calibration procedure (*5*). The typical modulation frequency was 45 Hz.

RESULTS AND DISCUSSION

Considerations for Quantitative PAS

Photoacoustic phase, ψ, and magnitude information, q_n, may be combined in a response function which is proportional to the bulk absorption coefficient multiplied by the thermal diffusion length for the sample, $\beta\mu_s$. This analysis assumes that the thermal and light-scattering properties of the sample are identical to those of the calibration standards which are prepared by

loading the γ-alumina surface with small amounts of K_2CrO_4. The supported metal oxide catalyst samples used in this study contain 0.5 to 24% of metal by mass. In order to determine the limits for which the PAS response function is linear with respect to sample absorptivity, the PAS response function was evaluated for dilutions of NiO. Nickel oxide was chosen instead of cobalt oxide because the absorptivities of the nickel materials are less than those of the corresponding cobalt materials; hence, larger fractions of nickel catalyst in diluted samples are required to achieve the same signal level as obtained for diluted cobalt catalyst samples. The calculated thermal diffusion length for NiO is smaller than that for alumina by a factor of 18. If change in the thermal properties of the samples is the dominant factor, then the magnitude and the phase function, $f(\psi) = 2/(\tan \psi - 1)$, are expected to show a negative deviation with increasing NiO percentage producing a negative deviation from linearity for the PAS response function. The scattering coefficient for the finely powdered NiO is expected to be larger than that for the γ-alumina substrate. If this factor is dominant, the PAS magnitude and phase function, $f(\psi)$, are expected to show a positive deviation with increasing NiO percentage, producing a positive deviation from linearity for the PAS response function.

The normalized photoacoustic magnitude versus percentage of NiO in γ-Al_2O_3 is shown for selected wavelengths in Fig. 1. From 0 to 10% of NiO the curves have the appearance of a typical magnitude response curve as the saturation limit is approached. However, from 11 to 20% of NiO the curves appear to seek a higher saturation limit. Similarly, the photoacoustic phase function at selected wavelengths versus percentage of NiO in γ-Al_2O_3, shown in Fig. 2, exhibits typical curve shapes up to about 11% of NiO. Beyond this point the phase function deviates from linearity in a positive direction. These data are combined in the PAS response function in Fig. 3. The PAS response function is linear with percentge of NiO in γ-Al_2O_3 up to 11% NiO with zero intercept. It is concluded that the deviation from linearity beyond 11% NiO is predominantly due to increased light scattering in the sample. The implication of this information for quantitative PAS of cata-

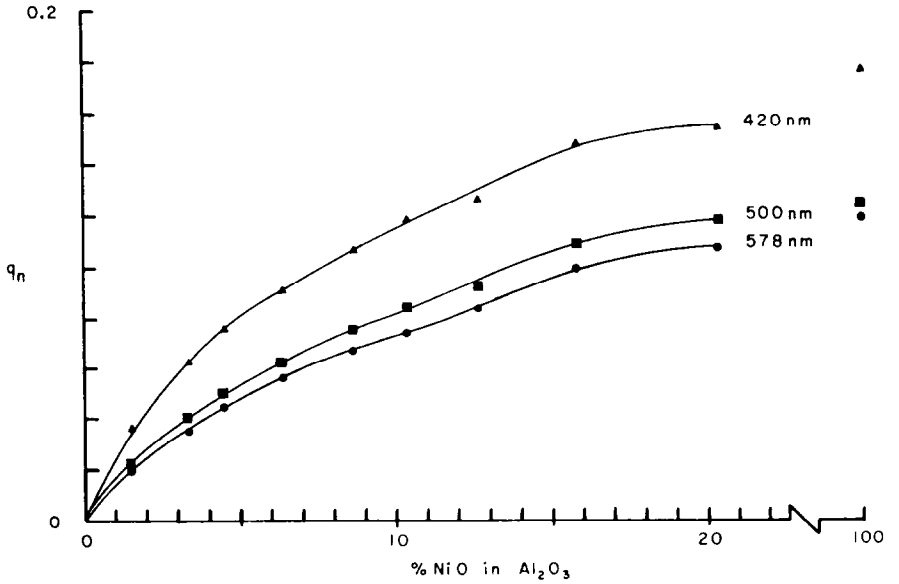

FIG. 1. Photoacoustic magnitude, q_n, versus percentage NiO in γ-Al_2O_3 for wavelengths 420, 500, and 578 nm.

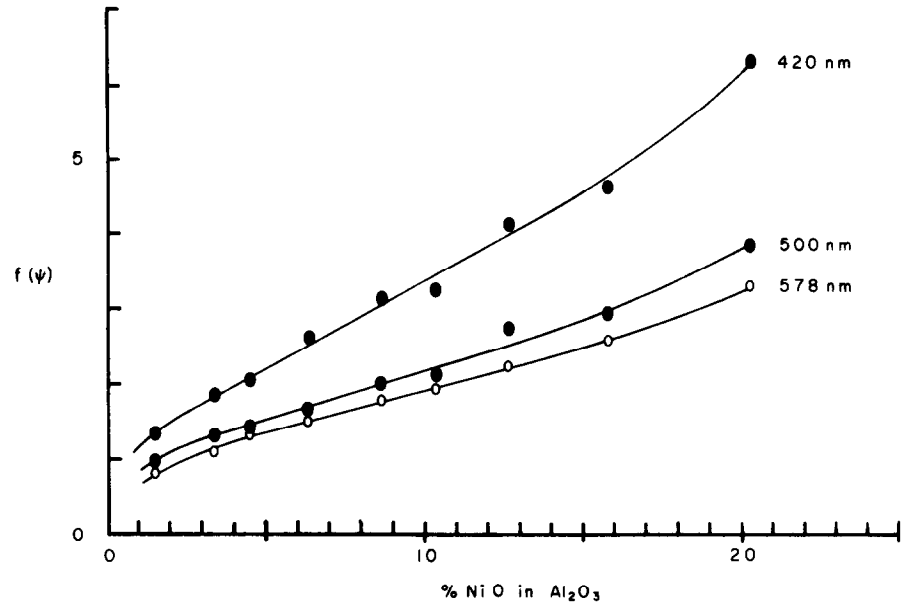

FIG. 2. Photoacoustic phase function, $f(\psi)$, versus percentage NiO in γ-Al_2O_3 for wavelengths 420, 500, and 578 nm.

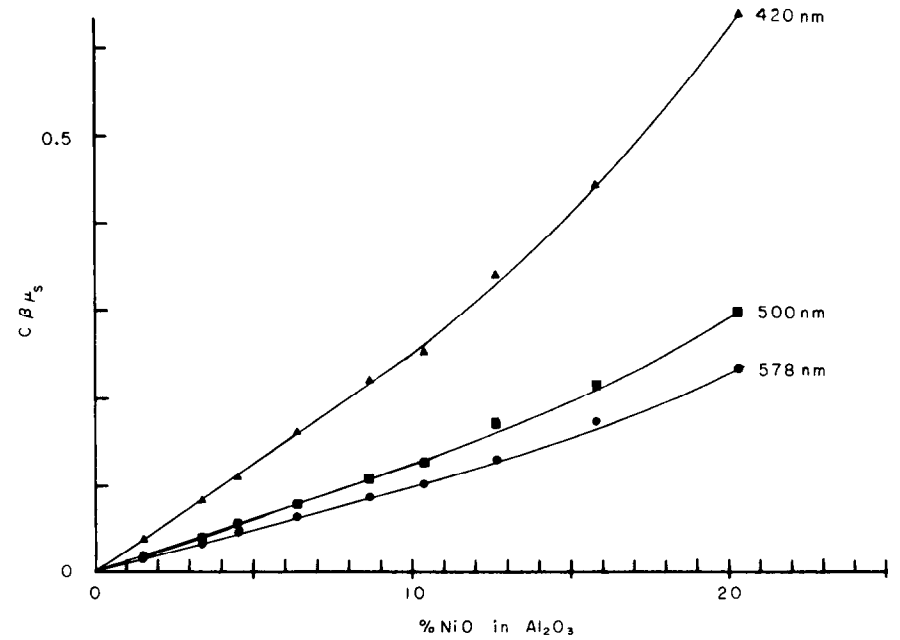

FIG. 3. Photoacoustic response function, $C\beta\mu_s$, versus percentage NiO in γ-Al_2O_3. The standard deviation at the 95% confidence limit and the correlation coefficient for a least-squares fit of the data up to 11% NiO are: 0.0047 and 0.9987 at 420 nm, 0.0012 and 0.9997 at 500 nm, 0.0012 and 0.9994 at 578 nm, respectively.

lysts is merely that the catalyst samples require sufficient dilution to limit the maximum NiO content of the samples to no more than 10%. It was found to be satisfactory to dilute the Ni catalyst samples having high metal loading to 10% Ni by mass for quantitative work. Cobalt catalyst samples were diluted to 0.5% Co by mass for quantitative work.

Nickel/γ-Alumina Catalysts

Surface spectroscopy summary. Metal-support interactions are known to influence the surface properties and, hence, the catalytic activity of alumina-supported metal catalysts. During calcination the metal ions diffuse into the first few atomic layers of the alumina lattice (0.1–0.4 nm) where they may occupy sites of tetrahedral or octahedral symmetry (*6*). At high metal loading a metal oxide species forms on the support surface. The octahedrally coordinated metal ions and the metal oxide species are readily reducible to the metal, while the tetrahedrally coordinated metal ions are not readily reduced and are catalytically inactive. The relative abundance and the distribution of these species depend on the metal loading and the calcination temperature.

Surface spectroscopy techniques showed that nickel strongly interacts with the γ-alumina support at low nickel loading (*1, 2*). The ESCA peak width for the Ni $2p_{3/2}$ line was correlated with the presence of two surface species: (1) nickel ions in surface sites of octahedral symmetry, Ni(O), and (2) nickel ions in surface sites of tetrahedral symmetry, Ni(T). As expected, increased calcination temperature was found to favor formation of the Ni(T) species because of enhanced diffusion into the γ-alumina lattice. Increased nickel loading favored formation of the Ni(O) species. The EXAFS results supported this interpretation (*3*). The average coordination number was found to increase from 4.8 to 5.3 as nickel loading increased from 2 to 15% in Ni/γ-Al_2O_3 catalysts calcined at 400°C. In the ESCA study of the Ni/γ-Al_2O_3 catalysts (*2*), the Ni/Al intensity ratio increased linearly with bulk nickel loading up to 17% nickel content. Beyond 17% nickel loading there was an enhancement of the Ni/Al ratio. This result was interpreted to mean that a separate phase (NiO) exists at the surface for nickel loading greater than 17%. After nickel saturates the surface sites, additional nickel contributes to an oxide phase on top of the substrate surface. The ISS Ni/Al intensity ratio showed a large increase beyond 20% nickel loading, consistent with the ESCA results. However, the intensity ratio exhibited a pronounced plateau between 10 and 17% nickel loading especially at high calcination temperature (600°C). This effect was attributed to the greater sensitivity of ISS to the depth distribution of Ni(T) and Ni(O) species. The ISS sampling depth is approximately 0.3 nm as compared to approximately 2 nm for ESCA. It has been proposed that nickel cations in tetrahedral surface sites tend to move below the surface where they are more shielded from the ion beam (*7*). The photoacoustic spectroscopy results are interpreted in terms of these ideas.

When Ni(II) is heated with γ-Al_2O_3 at very high temperatures $NiAl_2O_4$ is formed by incorporation of Ni(II) ions into the tetrahedral sites of the γ-alumina "defect" spinel structure (*8*). For a stoichiometric material at equilibrium, a disordered spinel structure is formed with about 22% of the Ni(II) ions in tetrahedral sites and the remainder in octahedral sites (*6*). Inversion occurs for the $NiAl_2O_4$ system because the energy preferences for octahedral sites over tetrahedral sites are not substantially different from Ni(II) and Al(III) (*9*). In Fig. 4 the visible photoacoustic spectra of a largely tetrahedral bulk $NiAl_2O_4$ spinel and a disordered bulk $NiAl_2O_4$ spinel structure are shown. The enhanced spectral features at 410–455 nm ($^3A_{2g} \rightarrow {}^3T_{1g}(P)$) and 650–715 nm ($^3A_{2g} \rightarrow {}^3T_{1g}(F)$) are due to octahedrally coordinated Ni(II) and the intense feature centered at about 610 nm ($^3T_1(F) \rightarrow {}^3T_1(P)$) is due to tetrahedrally

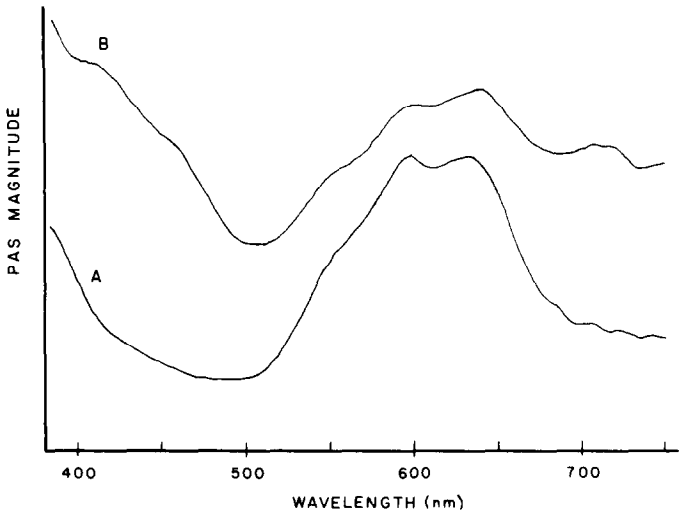

FIG. 4. Photoacoustic spectra of largely normal $NiAl_2O_4$ spinel (A) and disordered $NiAl_2O_4$ spinel (B).

coordinated Ni(II) (*10*). The photoacoustic spectrum of NiO exhibits the same characteristic octahedral absorption bands as the hexahydrate nickel ion and, additionally, a broad absorption in the region 500 to 600 nm which has been attributed to a Ni(III) charge transfer band (*11*).

Qualitative PAS results. Selected photoacoustic spectra of nickel catalysts which were calcined at 600°C are shown in Fig. 5. For nickel loadings less than 8% the spectrum is dominated by the Ni(T) surface species absorption. The expanded spectrum for the catalyst loaded with 2.5% nickel shows little evidence for octahedral nickel species. The $^3T_1(F) \rightarrow {}^3T_1(P)$ transition is shifted to shorter wavelength by approximately 6 nm as compared to the bulk Ni(T) spectrum shown in Fig. 4. The tetrahedral field is apparently slightly increased for sites near the surface. For nickel loadings between 7 and 20%, the absorption of the Ni(O) species makes an increasing contribution to the catalyst spectrum. Beyond 20% nickel loading, NiO is the dominant species adding to the absorption spectrum as evidenced by the increased absorption in the region 500 to 600 nm. At 24% nickel loading the Ni(T) spectrum is masked by NiO.

Photoacoustic spectra for selected Ni catalysts calcined at 500°C are shown in Fig. 6. In this case the octahedral nickel species make a substantial contribution even at 1.25% nickel loading. At 4% nickel loading the spectrum is dominated by absorption of octahedral species. These data are in agreement with the conclusion of Wu and Hercules (*2*) from ESCA studies that the ratio of Ni(T) to Ni(O) decreases with decreasing calcination temperature. At the lowest calcination temperature used, 400°C, the simple spectral assignments which were applied to the other nickel catalysts are no longer applicable. Spectral features centered at about 620 nm in the spectrum of the 1.25% nickel catalyst can be identified with Ni(T). However, the spectra for catalysts with less than 20% nickel are dominated by a broad visible absorption band which cannot be identified with the octahedral species, Ni(O) or NiO, or the tetrahedral species, Ni(T). Catalysts calcined at 400°C exhibit a broad absorption in the visible region with a structureless enhanced absorption at ~400 nm. This material is kinetically stable relative to NiO and Ni(O) as evidenced by the fact that heating the material in air at 600°C produces no appreciable change in the visible absorption

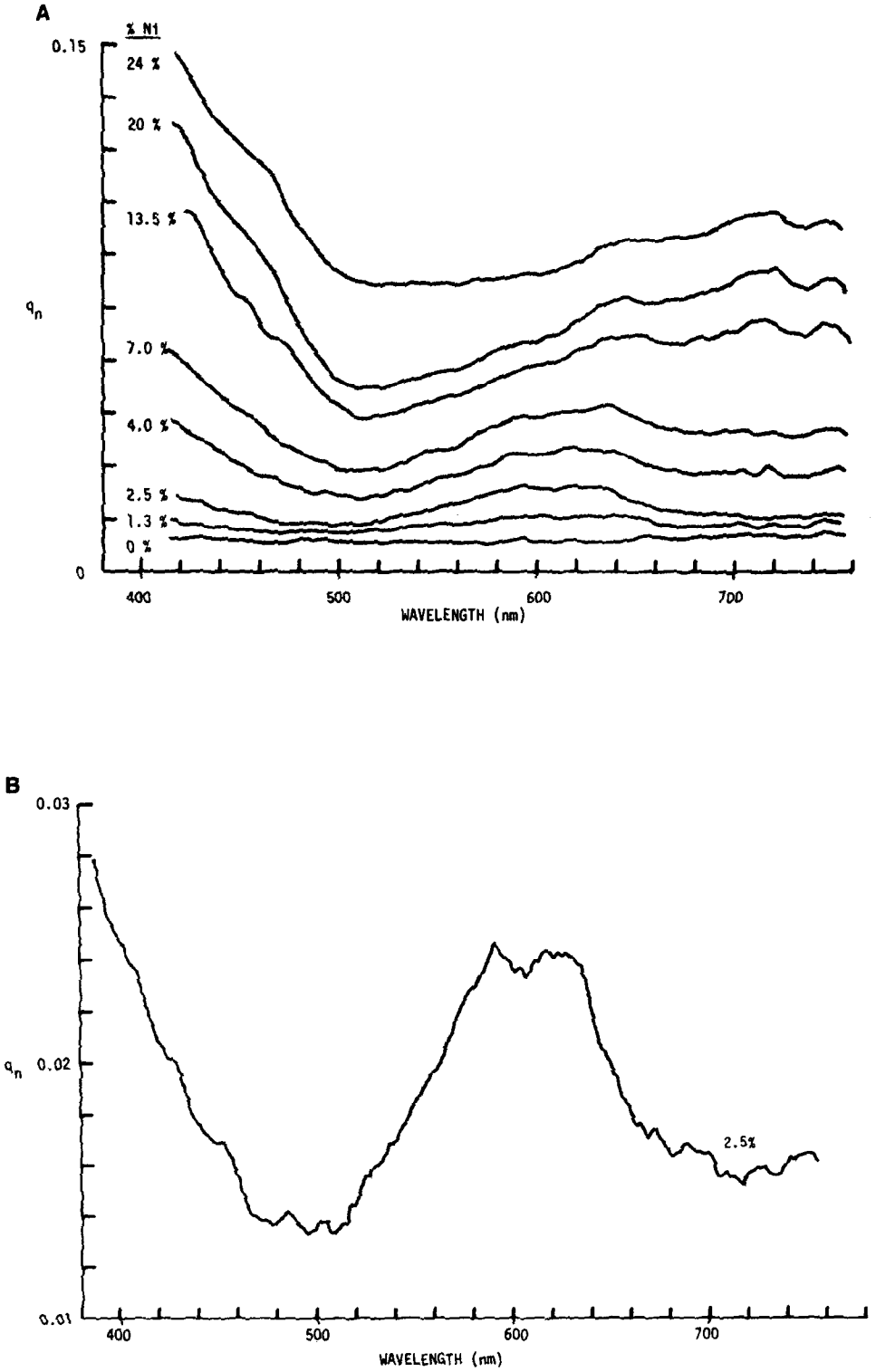

FIG. 5. Photoacoustic spectra of Ni/γ-Al_2O_3 catalysts calcined at 600°C: (A) full range of catalysts containing 0–24% Ni, (B) 2.5% Ni catalyst with *y* axis expanded.

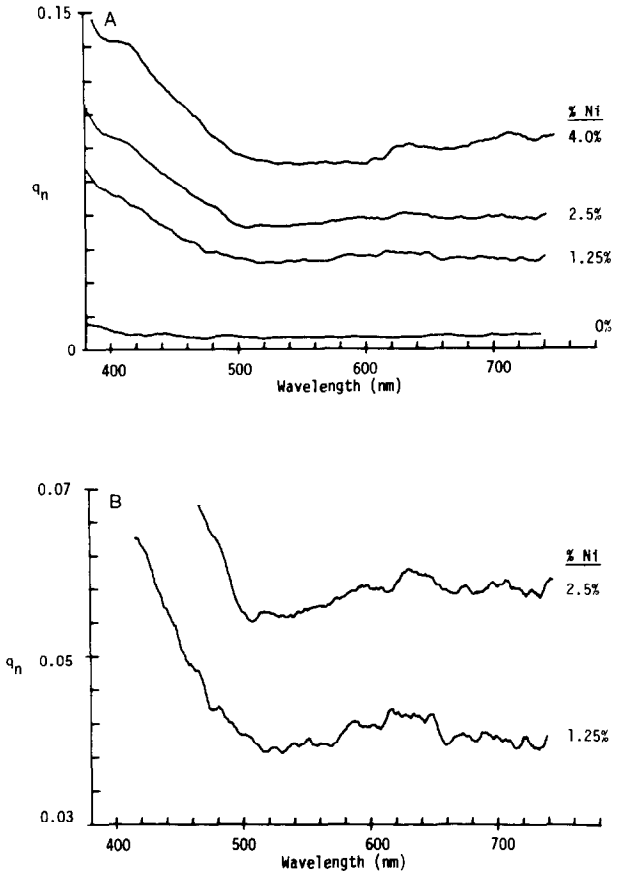

FIG. 6. Photoacoustic spectra of Ni/γ-Al_2O_3 catalysts calcined at 500°C.

spectrum. It is tempting to invoke the Ni(III) oxidation state to account for these spectra. The hypothesis of nickel species with an oxidation state greater than +2 on alumina surfaces was first proposed by Hill and Selwood (*12*) to account for average nickel valences between 2 and 3 found in reduction studies. This unusual stoichiometry is important only for nickel loadings less than 5% and for low calcination temperatures (*12, 13*). Stable gray-black nickel(III) hydroxides are known, whereas stable anhydrous nickel(III) oxides are not. Nickel(III) hydroxides have broad absorption bands and large absorptivities in the visible region, supporting this hypothesis. It is known that the presence of water influences the speciation in these materials (*6*). It is possible that the greater surface hydroxyl coverage in a humid, low-temperature preparation enhances the formation and stability of Ni(III) species. Current ESCA results have not yet supported or refuted this hypothesis. For high nickel loading of catalysts calcined at 400°C, spectral features appear which can be identified with octahedral nickel species.

Quantitative PAS results. As was pointed out earlier, NiO can be distinguished from the Ni(O) species by the broad absorption in the region 500 to 600 nm. At about 500 nm the absorption of the Ni(T) species exhibits a minimum; hence, the absorbance at 504 nm was selected to attempt to monitor NiO buildup. In Fig. 7 the photoacoustic response function at 504 nm divided by the percentage of nickel is plotted versus the bulk percentage of nickel

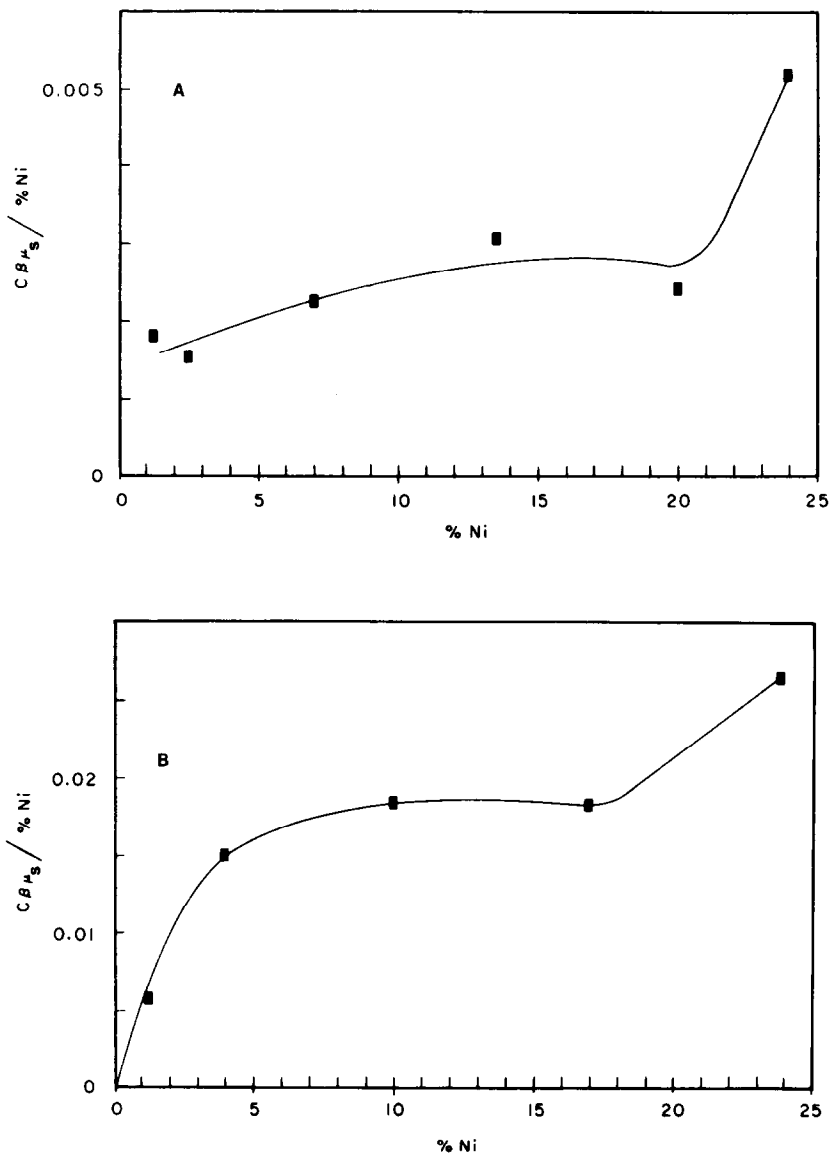

FIG. 7. Photoacoustic response function, $C\beta\mu_s$, at 504 nm divided by the percentage of nickel in the catalyst plotted versus the percentage of nickel for catalysts calcined at 600°C (A) and 400°C (B).

for catalysts calcined at 600 and at 400°C. In this type of plot the ordinate is proportional to the absorbance per unit percentage of metal on the surface. For both calcination temperatures a plateau is reached at about 10% nickel. The absorbance at the plateau is much higher for the 400°C calcination temperature due predominantly to the low-temperature absorber. In both cases, a large absorption enhancement occurs at about 20% nickel content. This is in good agreement with the Ni/Al intensity ratio results of ESCA and ISS which show enhancement beyond 17 and 20% nickel, respectively. In the case of the photoacoustic results also, this discontinuity can be associated with the segregation of a NiO phase on the alumina surface.

Measures of the absorbance due to Ni(T) and Ni(O) species on the surface which account for the NiO contribution to the absorption were devised. The estimated enhanced absorption of the tetrahedral nickel species above the absorption octahedral species is designated A_{590};

$$A_{590} = C\beta\mu_s(590) - \left[\frac{C\beta\mu_s(\mathrm{Ni},590)}{C\beta\mu_s(\mathrm{NiO},504)}\right] C\beta\mu_s(504), \quad (1)$$

where $C\beta\mu_s(590)$ and $C\beta\mu_s(504)$ are photoacoustic response functions for catalysts at 590 and 504 nm, respectively. $C\beta\mu_s(\mathrm{NiO},590)$ and $C\beta\mu_s(\mathrm{NiO},540)$ are photoacoustic response functions for NiO in γ-alumina at 590 and 504 nm, respectively, each determined by a linear least-squares fit as illustrated in the section dealing with considerations for quantitative PAS. Similarly, the enhanced absorbance at 450 nm, A_{450}, is a measure of the Ni(O) absorbance.

In Fig. 8, A_{590} and A_{590}/% Ni are plotted versus the percentage of nickel in catalysts calcined at 600°C. As expected, the fraction of nickel existing as Ni(T) is greatest at low nickel loading. This fraction diminishes smoothly to 20% nickel loading. At about 20% nickel content A_{590} shows a negative-going discontinuity. It is reasonable to suggest that the NiO phase which segregates at about 20% nickel loading optically masks the Ni(T) species thereby reducing the Ni(T) signal. This interpretation agrees well with a catalyst model for which a NiO phase is stabilized and supported on top of the nickel "surface spinel."

In Fig. 9, A_{450} and A_{450}/% Ni are plotted versus percentage of nickel for catalysts calcined at 600°C. Ni(O) is seen to contribute little to nickel loadings less than 5%, where the dominant species is Ni(T). The fraction of nickel existing as Ni(O) increases rapidly above 5% nickel loading. A_{450} does not show the discontinuity at 20% nickel content that A_{590} does. The qualitative interpretation of photoacoustic spectra for catalysts calcined at 600°C required reference only to Ni(T) and Ni(O) contributions for nickel loading up to 20%. The quantitative results are also consistent with the conclusion that Ni(O) and Ni(T) are the dominant species on the surface of these catalyst samples. Under this assumption the distribution ratio of Ni(T) to Ni(O) is found to vary from 1 : 0 for nickel loadings

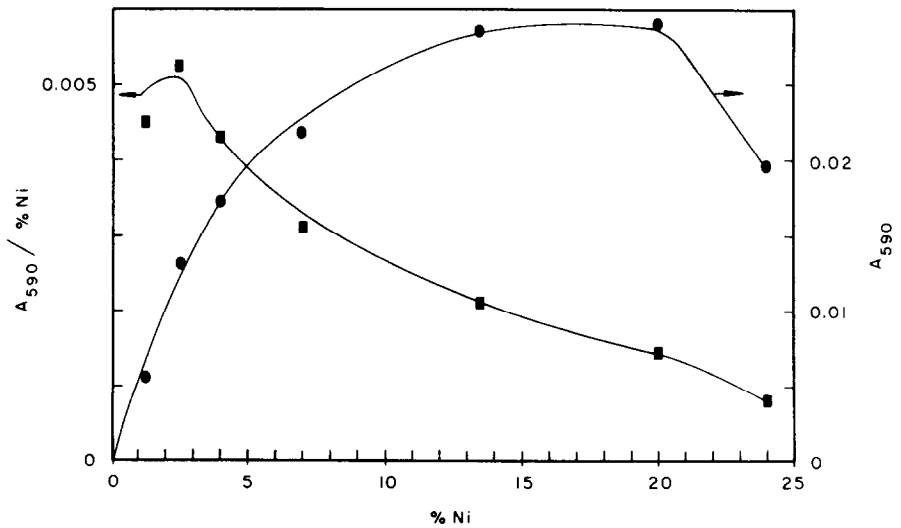

FIG. 8. Net photoacoustic response function at 590 nm, A_{590}, and A_{590}/% Ni plotted versus percentage of nickel in catalysts calcined at 600°C. ■—A_{590}/% Ni; ●—A_{590}.

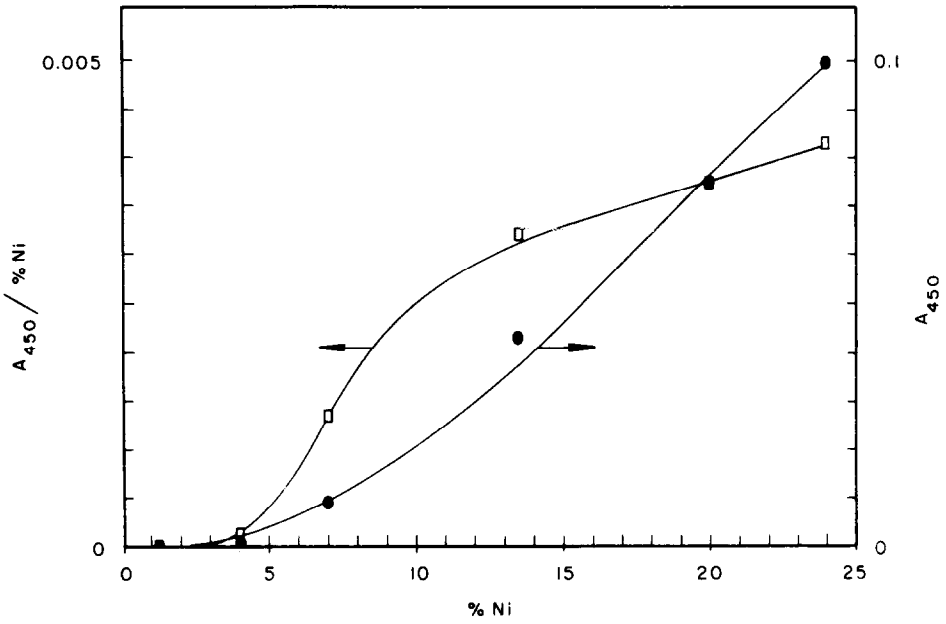

FIG. 9. Net photoacoustic response function at 450 nm, A_{450}, and A_{450}/% Ni plotted versus percentage of nickel in catalysts calcined at 600°C. □—A_{450}/% Ni; ●—A_{450}.

less than 3% to 0.3 : 0.7 for 20% nickel loading. The latter value is close to the bulk ratio for the inverted bulk $NiAl_2O_4$ spinel, 0.22:0.78 (*6*).

Several conclusions can be drawn from the photoacoustic spectroscopy study of impregnated Ni/γ-Al_2O_3 oxide catalysts correlated with surface spectroscopy results. First, PAS qualitative and quantitative results for 600°C are consistent with the presence of Ni(T) and Ni(O), the ratio of which varies from 1 : 0 for nickel loadings less than 3% to 0.3 : 0.7 for 20% nickel loading. The fraction of nickel existing as Ni(T) decreases with decreasing calcination temperature. Second, a nickel species exists on the surface having a spectrum not identified with Ni(T), Ni(O), or NiO for 400°C calcination temperature. Finally, NiO segregates on the surface above 20% nickel loading for catalysts calcined at 400 and 600°C.

Cobalt/γ-Alumina Catalysts

Surface spectroscopy summary. Surface spectroscopy investigations of the Co/γ-Al_2O_3 catalyst system have offered evidence for significant metal–support interaction. In ESCA spectra of these catalysts, the Co $2p_{3/2}$ line became less symmetrical and shifted to lower binding energy with increasing cobalt loading (*4*). At low cobalt content the peak shape and binding energy resembled those of the tetrahedral $CoAl_2O_4$ spinel, whereas, at high cobalt loading the peak shape and binding energy resembled those of Co_3O_4. The cobalt oxide, Co_3O_4, is a normal spinel oxide having Co(II) ions in tetrahedral interstices and an equal number of Co(III) ions in octahedral interstices (*14*, *15*). The ESCA Co 2*p* line of Co_3O_4 corresponds to an unresolved cobaltous–cobaltic doublet. As the cobalt loading on γ-alumina was increased the cobaltic line was enhanced. Higher calcination temperature favored formation of the tetrahedral cobaltous species, Co(T). Indirect evidence for octahedral cobalt on the catalyst surfaces was obtained from EXAFS (*3*). The average coordination number increased from 4.2 at 2% cobalt content to 5.2 at 16% cobalt content. (The average coordination number in Co_3O_4 is 5.3.) The ESCA Co/Al

intensity ratio increased gradually with metal loading up to 10% cobalt content. Above 10% cobalt loading the Co/Al intensity ratio was abruptly enhanced suggesting that a cobalt-rich layer is formed at the surface. The ISS Co/Al intensity ratio shows a similar discontinuity at about 12% cobalt content (*3*). The reduction studies showed a corresponding effect. The percentage reducibility of cobalt steadily increased with cobalt loading up to 12% cobalt loading, above which the increase was much less pronounced (*3*). A picture of cobalt speciation emerges in which Co(II) ions predominantly diffuse into tetrahedral γ-alumina surface sites at low cobalt loadings. As the cobalt concentration on the surface increases, Co(III) occupies octahedral surface lattice sites; and above 12% cobalt content Co_3O_4 segregates on the γ-alumina surfaces. Again, the photoacoustic spectroscopy results are interpreted in terms of these ideas.

Qualitative PAS results. Photoacoustic spectra of reference materials were recorded for comparison with catalyst spectra. In Fig. 10 selected spectra in the visible region of Co/γ-Al_2O_3 catalysts calcined at 600°C are shown. At 0.5% cobalt loading the spectrum is very similar to that of $CoAl_2O_4$ except that the Co(T) spectrum is shifted to shorter wavelengths by approximately 6 nm as compared to that of bulk $CoAl_2O_4$, just as in the case of the Ni/γ-Al_2O_3 system. Again, it is concluded that the surface tetrahedral sites experience a slightly larger ligand field at the surface of the γ-alumina than in the bulk material. For cobalt loadings larger than 1%, the catalyst spectrum is dominated by a spectrum similar to that of Co_3O_4. Above 12% cobalt content the visible catalyst spectrum is indistinguishable from that of Co_3O_4.

Unlike the Ni/γ-Al_2O_3 system, the spectral differences with calcination temperature are only differences of relative magnitude, not differences of kind. In the catalysts calcined at 400°C the Co(T) component is smaller than that for catalysts calcined at 600°C. A difference spectrum accentuates the effect of calcination temperature on catalyst spectra. In Fig. 11 a difference spectrum is shown for two catalysts loaded with 0.5% cobalt in which the spectrum of the catalyst calcined at 400°C is subtracted from the spectrum of the catalyst calcined at 600°C. The spectral feature labeled Co(O) is consistent with an assignment for the $^1A_{1g} \rightarrow {}^1T_{2g}$ transition of octahedrally coordinated Co(III). There is no evidence for octahedral Co(II). The assignments for Co(T) and Co(O) are in agreement with those made by Asmolov and Krylov in the diffuse reflectance spectroscopy study of the Co/γ-Al_2O_3 system (*16*).

Quantitative PAS results. In this case there are no visible spectral features which can be used to differentiate between Co(O) and Co_3O_4. However, the Co(O) feature is especially enhanced compared to the Co_3O_4 spectrum. As in the case of the Ni/γ-Al_2O_3 system, measures of the absorbance due to Co(T) and Co(O) species are determined. For example, the enhanced absorbance of Co(T) above the estimated absorbance of octahedral species is designated A_{578};

$$A_{578} = C\beta\mu_s(578) - \left[\frac{C\beta\mu_s(Co_3O_4,578)}{C\beta\mu_s(Co_3O_4,722)}\right] C\beta\mu_s(722), \quad (2)$$

where $C\beta\mu_s(578)$ and $C\beta\mu_s(722)$ are photoacoustic response functions for catalysts at 578 and 722 nm, respectively. $C\beta\mu_s(Co_3O_4,578)$ and $C\beta\mu_s(Co_3O_4,722)$ are photoacoustic response functions for Co_3O_4 in γ-alumina at 578 and 722 nm, respectively. The enhanced absorbance at 420 nm, A_{420}, associated with the Co(O) species is calculated in a similar way.

In Fig. 12, A_{578} and A_{578}/% Co are plotted versus percentage cobalt for catalysts calcined at 400 and 600°C. The amount of Co(T) reaches a plateau at about 2% cobalt content. The fraction of cobalt existing as Co(T) is greatest below 2% cobalt content. As expected, higher calcination temperature enhances Co(T) formation. The aver-

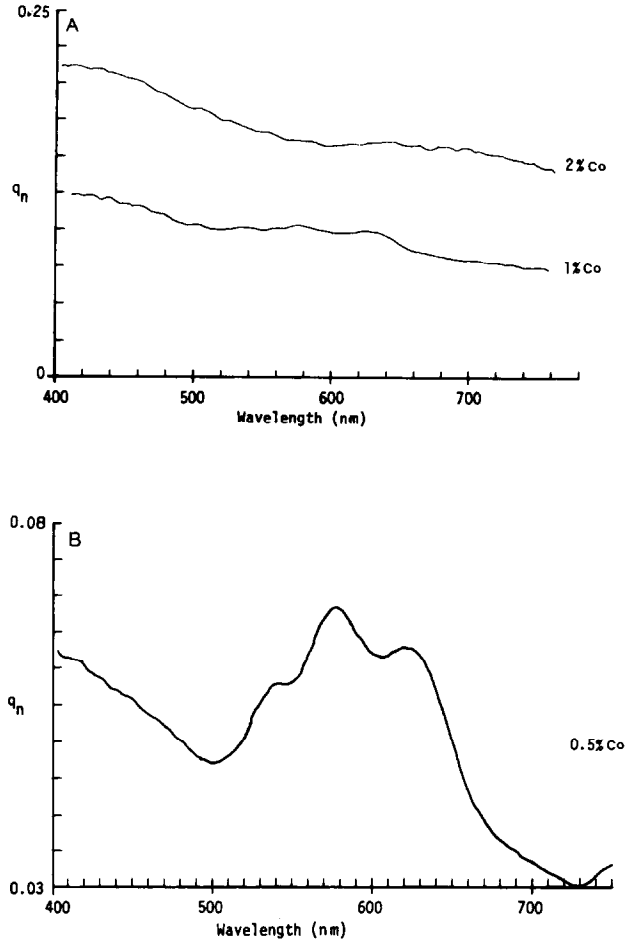

FIG. 10. Photoacoustic spectra of Co/γ-Alp$_2$O$_3$ catalysts calcined at 600°C: (A) 2 and 1% Co catalysts; (B) 0.5% Co catalyst.

age ratio of Co(T) formed at 600°C compared to that at 400°C is 0.70. From this ratio an approximate activation energy for Co(T) formation relative to the formation of Co(O) is calculated to be 2.1 kcal/mol. For catalysts calcined both at 400 and 600°C the Co(T) signal, A_{578}, decreases at 12% cobalt content. This suggests that the tetrahedral component is optically masked by the oxide phase at 12% cobalt content, analogous to the Ni/γ-Al_2O_3 system. This is in complete agreement with the interpretation of ESCA, ISS, and reduction studies (*4*).

In Fig. 13, A_{420} and A_{420}/% Co are plotted versus the percentage of cobalt in catalysts calcined at 400 and 600°C. There is little Co(O) formed for cobalt content less than 2% where Co(T) is greatest. The fraction of cobalt existing as Co(O) increases steadily up to approximately 2% cobalt content beyond which the fraction is insensitive to cobalt loading. At both calcination temperatures the quantity of Co(O) increases in a nearly linear way for cobalt loadings greater than 2%. This is in good agreement with reduction studies (*4*). The average ratio of Co(O) formed at 400°C compared to that at 600°C is 0.65. From this ratio an approximate activation energy for Co(O) formation relative to Co(T) formation is calculated to be −2.5 kcal/mol.

Assuming that Co(O) and Co(T) are the

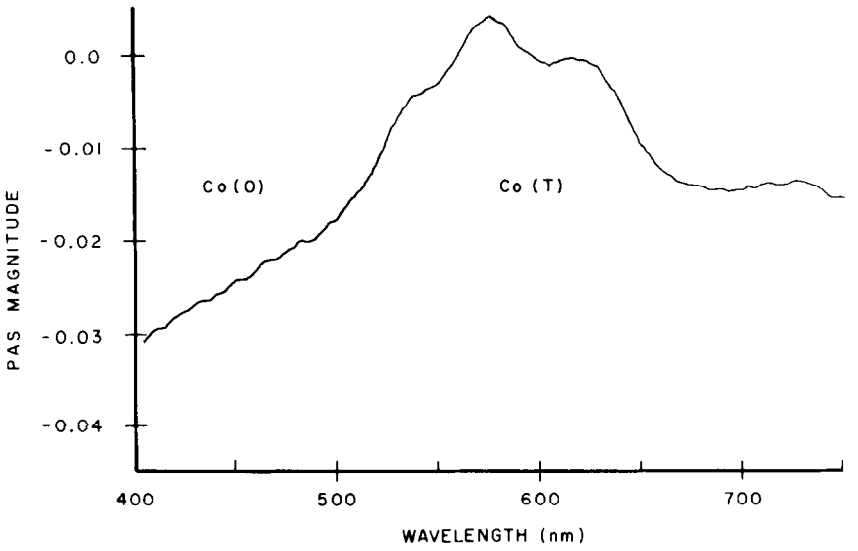

FIG. 11. Difference spectrum for 0.50% Co/γ-Al_2O_3 catalysts in which the spectrum of the catalyst calcined at 400°C is subtracted from that of the catalyst calcined at 600°C.

only species which make significant contribution to the visible absorption, the distribution ratio of Co(T) to Co(O) was found to vary from 09 : 0.1 for 0.5% cobalt content to 0.2 : 0.8 for 8.0% cobalt content at 600°C calcination temperature. For catalysts calcined at 400°C, the ratio of Co(T) to Co(O) was found to vary from approximately 0.8 : 0.2 for 0.5% cobalt content to 0.1 : 0.9 for 8.0% cobalt content. However, the data suggest that, unlike the Ni/γ-Al_2O_3 system, the Co(O) and Co(T) species cannot account for the total cobalt loading in this concentration range. A report (*17*) of Co_3O_4 detected by X-ray diffraction on Co/γ-Al_2O_3 catalysts with cobalt content as low as 2% suggests a contribution from oxide material.

Several conclusions are supported by the PAS study of impregnated Co/γ-Al_2O_3 oxide catalysts, correlated with surface spectroscopy. First, spectral features in the visible photoacoustic spectra can be identified with tetrahedral Co(II), designated Co(T), and octahedral Co(III), designated Co(O). The Co(T)-to-Co(O) ratio in Co/γ-Al_2O_3 catalysts is consistently larger for catalysts calcined at 600°C as compared to those calcined at 400°C. An apparent activation energy for Co(T) formation relative to Co(O) formation is approximately 2.3 ± 0.5 kcal/mol. Second, the ratio of Co(T) to Co(O) diminishes steadily with increasing cobalt loading. For 600°C calcination temperature, the Co(T)-to-Co(O) ratio varies from approximately 0.9 at 0.5% cobalt content to approximately 0.25 at 8.0% cobalt content. Finally, masking of the Co(T) signal at 12% cobalt content is associated with Co_3O_4 segregation on the catalyst surface.

Cobalt–Molybdenum/γ-Alumina Catalysts

Background. The role of cobalt in Co–Mo/γ-Al_2O_3 hydrodesulfurization catalysts is not known with certainty. It is known that various molybdenum compounds are catalytically active in the desulfurization process while cobalt compounds which contain no molybdenum are not catalytically active. However, the presence of cobalt enhances the catalytic activity. The most active catalysts are those prepared by impregnation of alumina with solutions of ammonium molybdate and a cobalt salt, followed by drying and calcining.

For the purpose of studying cobalt interaction with the alumina support and molybdenum, a series of Co–Mo/γ-Al_2O_3

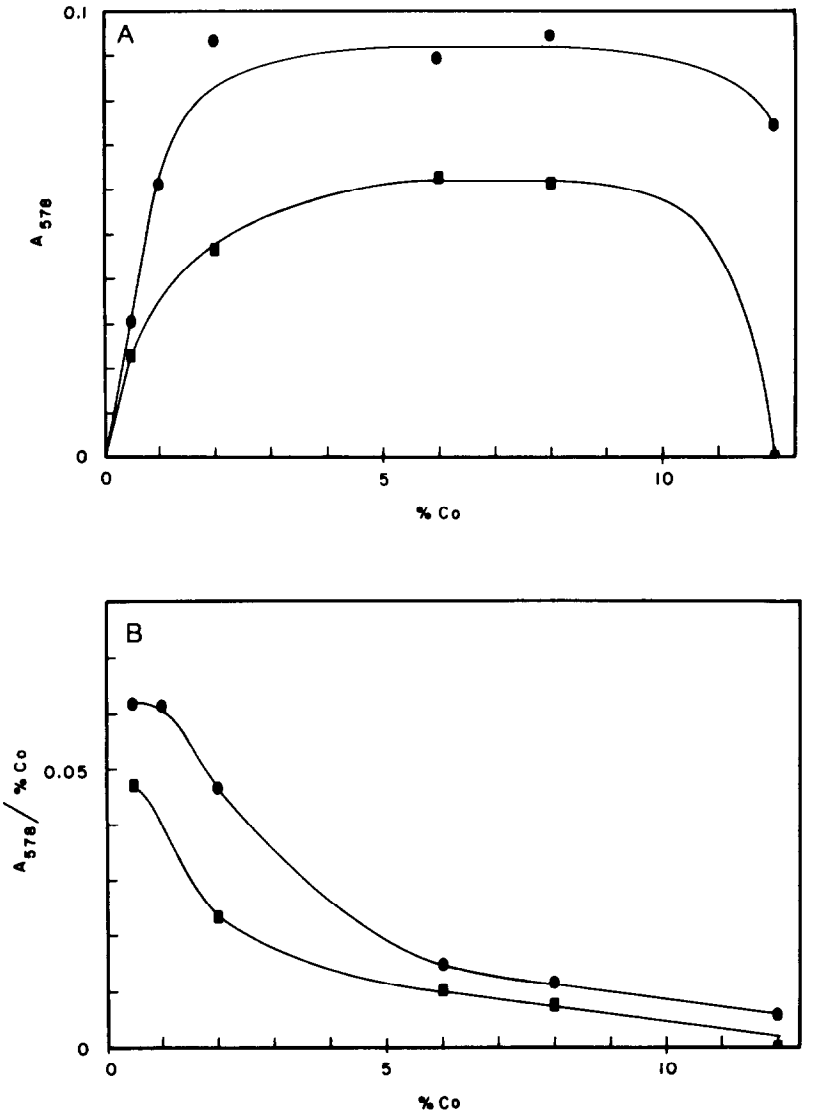

FIG. 12. Net photoacoustic response function at 578 nm, A_{578} (A), and A_{578}/% Co (B) plotted versus percentage of cobalt in catalysts calcined at 400°C (■) and 600°C (●).

catalysts were prepared by sequential impregnation of γ-Al_2O_3 with molybdenum and cobalt. All the catalysts in this series were first loaded with molybdenum, 15% molybdenum as MoO_3. (The final molybdenum loading on the catalysts was found to be 14.2% molybdenum as MoO_3.) Calcining this material produces what is believed to be a Mo monolayer on the alumina surface (*17*). Samples of molybdenum-loaded alumina were impregnated with various amounts of cobalt nitrate and calcined. The competition between the cobalt interaction with the MoO_3 layer and the γ-Al_2O_3 support was of interest.

Qualitative PAS results. The visible photoacoustic spectrum of $CoMoO_4$ is characterized by an absorption maximum centered at about 570 nm, with spin–orbit splitting features at about 528, 560, and 584 nm. These spectral features are sufficiently well separated from the spin–orbit triplet of

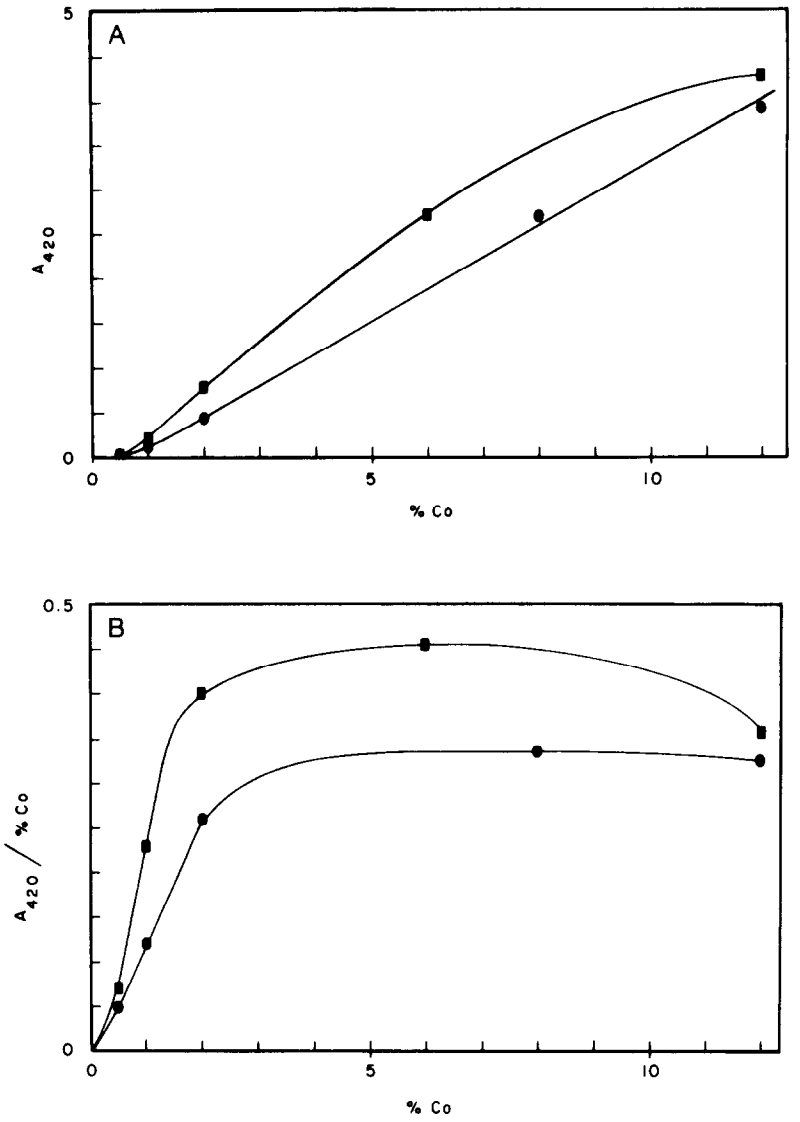

FIG. 13. Net photoacoustic response function at 420 nm, A_{420} (A) and A_{420}/% Co (B) plotted versus percentage of cobalt in catalysts calcined at 400°C (■) and 600°C (●).

Co(T) to permit a qualitative statement about which cobalt species is dominant in the visible spectrum. At 7% cobalt the spectrum becomes dominated by the broadband absorbance of Co_3O_4 just as for large cobalt loading of γ-Al_2O_3 alone. For cobalt loadings less than 7% the spectrum resembles that of the Co(T) spinel. There is no evidence for Co(O) buildup. For 0.8% cobalt the spectrum appears to be intermediate between that of a surface spinel and that of a bulk spinel. Although this evidence is not conclusive, it is possible that Co(T) is buried beneath the MoO_3 phase. This would also reduce formation of Co(O) at the surface. At 5.5% cobalt loading minor spectral features are observed which are correlated with the $CoMoO_4$ spin–orbit features. The Co–Mo oxide is, however, not a major constituent. The presence of a MoO_3 monolayer prevents formation of octahedral Co^{3+} at the support surface.

On the basis of a comparison of the Co–Mo/γ-Al_2O_3 system with the Co/γ-Al_2O_3 system it is concluded that the dominant form of cobalt at low cobalt loading is Co(T) in both systems. In the case of Co–Mo/γ-Al_2O_3 there is evidence that the Co(T) species is not formed as close to the support surface as in Co/γ-Al_2O_3.

At very high Co loading an oxide phase is formed which masks other spectral features.

The presence of Mo inhibits the formation of Co(O); instead, there is evidence for formation of a small amount of a cobalt–molybdenum oxide.

Model for Metal–Support Interactions

The phenomenon of metal–support interactions as a function of metal loading and calcination temperature for Ni/γ-Al_2O_3 and Co/γ-Al_2O_3 catalysts has been described. A simple model is advanced here to account for the qualitative dependence of surface speciation on metal loading and calcination temperature in these catalysts.

Mixed metal oxides, $M^{II}M_2^{III}O_4$, often have a spinel structure based on a cubic close packed array of oxide ions in which one-eighth of the tetrahedral holes (two per anion) are occupied by M^{II} ions and one-half of the octahedral holes (one per anion) are occupied by M^{III} ions. This arrangement is designated $M^{II}[M_2^{III}]O_4$, where the square brackets enclose the ions which occupy octahedral interstices. Other mixed metal oxides take on an inverse spinel structure, $M^{III}[M^{II}M^{III}]O_4$, in which the M^{II} ions occupy octahedral interstices instead of tetrahedral interstices. In disordered spinels, i.e., partially inverted spinels, a fraction of M^{II} ions occupy tetrahedral interstices (*18*). The degree of inversion, x, in the hypothetical reaction in Eq. (3) has been related to a site preference energy for various transition metal ions relative to Al^{3+} in Al_2O_3 (*9*). The values of x and the interchange enthalpy for $NiAl_2O_4$ are 0.78 and -2 kcal, respectively; the corresponding values for $CoAl_2O_4$ are 0.05 and +13 kcal.

$$M^{II}[M_2^{III}]O_4 \rightarrow M^{II}_{1-x}M^{III}_x[M^{II}_xM^{III}_{2-x}]O_4. \quad (3)$$

The catalyst support is a spinel structure which can be represented by $Al_{2/3}\,\square_{1/3}\,[Al_2]O_4$. The formation of M(T) can, therefore, be represented by diffusion of M^{II} into these lattice vacancies.

$$M^{II} + 3\ Al_{2/3}\square_{1/3}[Al_2]O_4 \rightarrow 3\ Al_{2/3}M_{1/3}[Al_2]O_4. \quad (4)$$

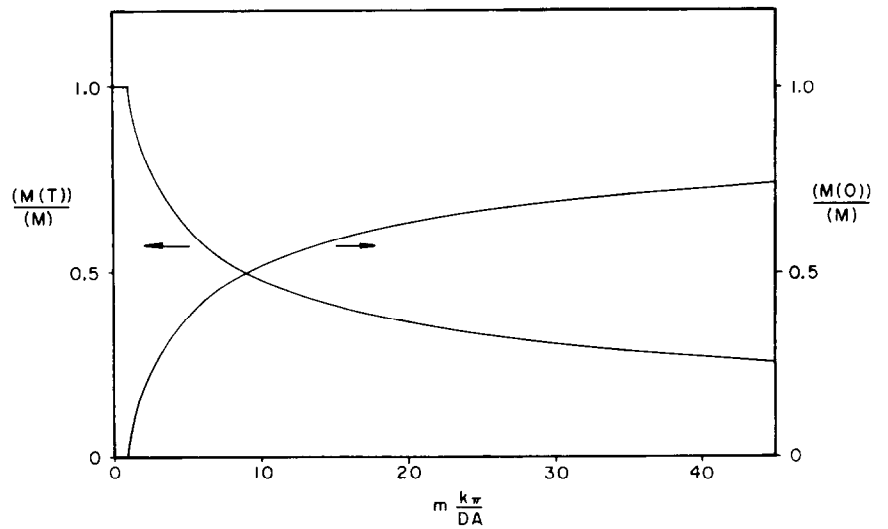

FIG. 14. Model prediction of relative amounts of M(T) and M(O) versus metal loading, represented by $mk_i\pi/DA$.

The formation of M(O) can similarly be described as inversion of these M(T) sites.

$$3\ Al_{2/3}M_{1/3}[Al_2]O_4 \rightarrow 3\ Al[M\ Al_{5/3}]O_4. \quad (5)$$

For M(O) formation, there is a net exchange of an Al^{3+} from an octahedral position to a tetrahedral position. The activation energy for this process is expected to be higher than that for M(T) formation. Navrotsky and Kleppa (*9*) report the octahedral site preference energy for Al^{3+} to be 10.6 kcal/mol. The Tammann temperature for bulk lattice mobility in alumina (melting point = 2015°C) is approximately 870°C (*19*). Hence, it is surmised that the inversion process is slow at the calcination temperatures used in this study. This conjecture is supported by experiment. After calcining a Ni/γ-Al_3O_3 sample (4% Ni, 600°C) for an additional 54 h at 600°C, no detectable change in the M(T)/M(O) ratio was observed. However, this is not expected to be the case for the inversion process at the surface where the activation energy will be less. Surface diffusion is often important at a much lower temperature than bulk diffusion (*20*). The Tammann temperature for surface mobility in alumina is approximately 410°C. This phenomenon is very dependent on the surface history. A model for speciation in these catalysts is developed based on an inversion process important only at the surface of the γ-Al_2O_3 support.

A hypothetical model for speciation at the γ-Al_2O_3 surface is given in Eq. (6).

$$\begin{array}{ccc} M_S & & \\ \downarrow & & \\ M_S(T) & \overset{k_i}{\rightleftharpoons} & M_S(O) \\ \Big\downarrow D & & \Big\downarrow D_0 \\ M_B(T) & \rightleftharpoons & M_B(O). \end{array} \quad (6)$$

Within seconds of beginning calcination of a γ-Al_2O_3 sample impregnated with a small amount of $Ni(NO_3)_2$ or $Co(NO_3)_2$, the sample takes on a gray color as the nitrate is decomposed. The gray color slowly gives way to the blue color of M(T). The gray material, M_S, which is initially formed may be an amorphous metal oxide bound on the surface. The first step involves incorporation of metal ions into available tetrahedral defect sites on the surface. $M_S(T)$ is removed from the surface by inversion to M(O), with rate $k_i[M_S(T)]$, or by diffusion into the bulk γ-Al_2O_3 lattice which is characterized by a diffusion coefficient, D. It is assumed that inversion does not occur in the bulk alumina at the calcination temperatures used. The rate of diffusion of M(O) into the bulk is expected to be much smaller than that for M(T). If a vacancy diffusion model is involved then M(O) diffuses via thermally created lattice vacancies as opposed to defect lattice vacancies. Interstitial and exchange diffusion mechanisms are expected to have higher activation energies than a vacancy diffusion mechanism (*21*). When the lattice near the surface becomes saturated with M(O) and M(T) both diffusion and inversion processes slow and growth of microcrystals of metal oxide accounts for the remaining metal. The arguments used to justify this model are made referring only to an inversion reaction at the surface. In Table 1 surface reaction assignments are proposed for the three catalyst systems studied.

Simple competition between inversion of the spinel forming $M_s(O)$ at the surface and diffusion of M(T) into the bulk of the γ-Al_2O_3 spinel is envisaged. If a steady-state concentration, C_T, or $M_s(T)$ is assumed, then the rate of removal of $M_s(T)$ from the surface by diffusion is given by

$$\text{diffusion rate} = C_T \left(\frac{DA}{\pi t}\right)^{1/2}, \quad (7)$$

where A is the area of the surface and t is the time. The rate of removal of $M_s(T)$ from the surface by inversion is

$$\text{inversion rate} = k_i C_T. \quad (8)$$

The approximate time required to incorporate the metal into the lattice is related to

TABLE 1

Assignments for Application of the Interaction Model to Catalyst Systems

System	$M_s(T)^a$	$M_B(T)^b$	M(O)	$M_s(T) \xrightarrow{k} M(O)$
Ni/γ-Al_2O_3	Ni^{2+}	Ni^{2+}	$Ni^{2+}(O)$	$Ni_s^{2+}(T) \rightarrow Ni_s^{2+}(O)$
Co/γ-Al_2O_3	Co^{2+}	Co^{2+}	$Co^{3+}(O)$	$Co_s^{2+}(T) \rightarrow Co_s^{3+}(O)$
Co–Mo/γ-Al_2O_3	Co^{2+}	Co^{2+}	Co–Mo oxide ($CoMoO_4$)	$Co_s^{2+}(T) \rightarrow CoMoO_4$

[a] Surface tetrahedral sites.
[b] Bulk tetrahedral interstices.

the metal loading by

$$(M)_{total} - \left[2\left(\frac{DA}{\pi}t\right)^{1/2} + k_i t\right] C_T. \quad (9)$$

The relative amounts of metal incorporated into tetrahedral interstices and octahedral interstices are given by Eqs. (10) and (11), respectively.

$$\frac{(M_B(T))}{(M)} = \frac{2}{1 + (1 + m(k_i\pi/DA))^{1/2}}. \quad (10)$$

$$\frac{(M_B(O))}{(M)} = \frac{(1 + m(k_i\pi/DA))^{1/2} - 1}{1 + (1 + m(k_i\pi/DA))^{1/2}}. \quad (11)$$

In these relationships m is given by

$$m = \frac{(M)}{C_T}. \quad (12)$$

The relative amounts of M(T) and M(O) are plotted versus the metal loading as represented by $mk_i\pi/DA$ in Fig. 14. An induction period corresponding to $k_i\pi/DA$ is included for achieving steady state. Formation of M(T) dominates at low metal loading and M(O) formation dominates at high metal loading. Even for this crude model, the predicted dependence of the formation of tetrahedral and octahedral species on metal loading is very similar to the corresponding experimental curves for Ni/γ-Al_2O_3 and Co/γ-Al_2O_3 in Figs. 8 and 9 and 12 and 13, respectively. This model predicts that the relative amount of M(T) compared to M(O) varies with temperature: $a \exp(E_i - E_d)/RT$, where E_i is the activation energy for inversion at the surface and E_d is the activation energy for diffusion of M(T) into bulk alumina. It has been shown that M(T) increases at the expense of M(O) with increasing temperature. On the basis of the model, it is expected that the relative quantity of M(T) to M(O) increases with temperature as $E_d > E_i$ for inversion in the bulk lattice. This is another reason to believe that only inversion at the substrate surface is significant.

CONCLUSIONS

Photoacoustic spectroscopy provided useful information on metal–support interactions in alumina-supported catalysts. The PAS studies on Ni/γ-Al_2O_3, Co/γ-Al_2O_3, and Co–Mo/γ-Al_2O_3 oxide catalysts are in good agreement with previous surface spectroscopy results. The results are consistent with a model which describes competition between formation of a tetrahedral species, M(T), by diffusion of the metal ion into the γ-Al_2O_3 spinel and formation of an octahedral species, M(O), only at the support surface. When neither of these processes is important, metal oxide is formed on the surface. This mechanism satisfactorily accounts for the dependence of the M(T)/M(O) ratio on metal loading and calcination temperature in the Ni/γ-Al_2O_3 and Co/γ-Al_2O_3 catalyst systems.

ACKNOWLEDGMENTS

This research was supported in part by the U.S. Department of Energy under Grant DE-AC02-79ER10485.A00 (D.M.H., R.L.C.) and by a grant from the AMAX Foundation (D.E.L.). L.W.B. thanks to the Air Force Institute of Technology for their support.

REFERENCES

1. Wu, M., Chin, R. L., and Hercules, D. M., *Spectrosc. Lett.* **11,** 615 (1978).
2. Wu, M., and Hercules, D. M., *J. Phys. Chem.* **83,** 2003 (1979).
3. Greegor, R. B., Lytle, F. W., Chin, R. L., and Hercules, D. M., *J. Phys. Chem.* **85,** 1232 (1981).
4. Chin, R. L., and Hercules, D. M., *J. Phys. Chem.* **86,** 360 (1982).
5. Burggraf, L. W., and Leyden, D. E., *Anal. Chem.* **53,** 759 (1981).
6. Jacono, M. L., Schiavello, M., and Cimino, A., *J. Phys. Chem.* **75,** 1044 (1971).
7. Shelef, M., Wheeler, M. A. Z., and Yao, H. C., *Surf. Sci.* **47,** 697 (1975).
8. Richardson, J. T., and Milligan, W. O., *J. Phys. Chem.* **60,** 1223 (1956).
9. Navrotsky, A., and Kleepa, O. J., *J. Inorg. Nucl. Chem.* **29,** 2701 (1967).
10. Cotton, F. A., and Wilkinson, G., "Advanced Inorganic Chemistry," 2nd ed., pp. 881–885. Interscience, New York, 1967.
11. Klier, K., *Catal. Rev.* **1**(2), 207 (1967).
12. Hill, F. N., and Selwood, P. W., *J. Amer. Chem. Soc.* **71,** 2522 (1949).
13. Holm, V. C. F., and Clark, A., *J. Catal.* **11,** 317 (1968).
14. Cotton, F. A., and Wilkinson, G., "Advanced Inorganic Chemistry," 2nd ed., p. 891. Interscience, New York, 1967.
15. Cotton, F. A., and Wilkinson, G., "Advanced Inorganic Chemistry," 2nd ed., p. 864. Interscience, New York, 1967.
16. Asmolov, G. N., and Krylov, O. V., *Kinet. Catal.* **12,** 403 (1971).
17. Massoth, F. E., *in* "Advances in Catalysis and Related Subjects," Vol. 27, p. 265. Academic Press, New York/London, 1978.
18. Cotton, F. A., and Wilkinson, G., "Advanced Inorganic Chemistry," 2nd ed., p. 51. Interscience, New York, 1967.
19. Garner, W. E., "Chemistry of the Solid State," p. 307. Butterworths, London, 1955.
20. Adamson, A. W., "Physical Chemistry of Surfaces," 2nd ed., p. 265. Interscience, New York, 1967.
21. Manning, J. R., "Diffusion Kinetics for Atoms in Crystals," Chap. 1. Van Nostrand, Princeton, N.J., 1968.